CHEMPHYSCHEM

DOI: 10.1002/cphc.200900942

Planar Au/TiO_2 Model Catalysts: Fabrication, Characterization and Catalytic Activity

Menhild Eyrich,[a] Stefan Kielbassa,[a] Thomas Diemant,[a] Johannes Biskupek,[b] Ute Kaiser,[b] Ulf Wiedwald,[c] Paul Ziemann,[c] and Joachim Bansmann*[a]

Dedicated to Prof. Dr. R. Jürgen Behm on the occasion of his 60th birthday

Different types of planar Au/TiO_2 model catalysts are produced on TiO_2(110) single-crystal substrates and thin TiO_2 films on Ru(0001) by physical vapor deposition of gold under ultrahigh-vacuum (UHV) conditions or by micelle-based chemical routes. Both the Au nanoparticles and the support are characterized by surface-science-based methods (such as atomic force microscopy and X-ray photoelectron spectroscopy) as well as by transmission electron microscopy. Finally, the activity of the model catalysts in the CO oxidation reaction is analyzed in a microflow reactor. Au/TiO_2(110) model catalysts with a stoichiometric TiO_2(110) support exhibit only a low catalytic activity compared to those with a reduced crystal and Au/TiO_2 model catalysts with thin TiO_2 films on Ru(0001) as a substrate. The possible influence of Ti interstitials in the reduced TiO_2(110) substrates on the CO oxidation activity is discussed.

1. Introduction

Since the pioneering work by Haruta in the late 1980s,[1] supported Au catalysts have attracted much attention due to their unusual catalytic activity. For example, the oxidation of CO is possible at temperatures far below 100 °C (for an overview, see refs. [2,3]). In spite of numerous experimental and theoretical efforts with sometimes contradictory results (e.g., importance of metallic,[4,5] oxidic,[6,7] non-metallic[8] Au species, Au particles of bilayers height[9]), a detailed understanding of the CO oxidation reaction is still missing. It is generally accepted that not only the Au nanoparticles but also the nature of the support material influences the catalytic activity considerably, and—among others—also TiO_2 was discussed as "active support material".[10] Recently, it was suggested that a modification of the chemical and physical properties of the TiO_2 support can affect the catalytic activity,[11,12] and that the TiO_2 support might be more than a spectator in the reaction. The up to now unsolved mechanism might also be related to the possibility that differently prepared (powder as well as model) Au/TiO_2 catalysts indeed follow different reaction pathways. Recently, a discussion was started about the influence of oxygen vacancies and Ti interstitials on the catalytic activity of planar Au/TiO_2 model systems. New results indicate that oxygen surface vacancies are, from an energetic point of view, less important for the catalytic activity due to their instability in reactive gases compared to Ti interstitials.[13,14] Segregation of Ti interstitials from the bulk to the surface and formation of additional layers (see e.g., refs. [15,16]), which is characteristic for reduced titania, might play an important role in the heterogeneous catalysis of gold.

Due to their reduced structural complexity, planar Au/TiO_2 model catalysts have been widely used to get a better understanding of the fundamental principles of their catalytic activity. Since surface-science-based experimental methods, especially scanning tunneling microscopy (STM) and other electron-based techniques, often require an appropriate electrical conductivity of the substrate, reduced rutile TiO_2(110) substrates or (ultra)thin TiO_2 films on metal surfaces (mostly refractory materials such as Mo, Re) have been used for the respective experiments. Reduced (as well as afterwards re-oxidized) and stoichiometric TiO_2(110) substrates possess quite different chemical and physical properties (not only in their electric conductivity) and are expected to show different behaviors as model catalysts in combination with Au. Apart from a different ability of both surfaces to adsorb oxygen,[17–20] also the binding strength of Au atoms on the stoichiometric TiO_2(110) surface is significantly smaller compared to the reduced surface.[21] The higher density of defects on the reduced surface and the higher binding strength are responsible for different particle sizes on reduced and oxidized surfaces after evaporation of Au.[22,23]

Herein, we report on the structural and electronic properties of differently prepared Au/TiO_2 model catalysts and their catalytic activity. The first part of the manuscript is related to the

[a] M. Eyrich, Dr. S. Kielbassa, Dr. T. Diemant, Dr. J. Bansmann
Institut für Oberflächenchemie und Katalyse
Universität Ulm, Albert-Einstein-Allee 47
89081 Ulm (Germany)
Fax: (+49) 731-50-25452
E-mail: joachim.bansmann@uni-ulm.de

[b] Dr. J. Biskupek, Prof. Dr. U. Kaiser
Materialwissenschaftliche Elektronenmikroskopie
Universität Ulm, Albert-Einstein-Allee 11
89081 Ulm (Germany)

[c] Dr. U. Wiedwald, Prof. Dr. P. Ziemann
Institut für Festkörperphysik
Universität Ulm, Albert-Einstein-Allee 11
89081 Ulm (Germany)

TiO_2 support, namely, thin TiO_2 films on Ru(0001) as well as stoichiometric and reduced TiO_2(110) substrates, the second part to the corresponding properties of Au nanoparticles on these supports, and finally, their catalytic activity in the CO oxidation reaction is addressed. The data will be discussed with respect to other Au/TiO_2 model catalysts and theoretical models.

2. Results and Discussion

2.1. Structural, Electronic and Chemical Characterization of Planar Au/TiO_2 Model Catalysts

In our experiments on planar Au/TiO_2 model catalysts, Au has mainly been thermally evaporated in situ onto fully oxidized and bulk-reduced TiO_2(110) substrates and TiO_2 films on Ru(0001). Moreover, Au/TiO_2 samples have been produced ex situ by using the micelle-deposition technique. Since the support as well as the Au nanoparticles have an influence on the catalytic activity, both parts of the model catalysts are characterized regarding their geometric and electronic/chemical structure.

Structure of the TiO_2 Substrates

The surface topology of the differently prepared titania surfaces is displayed in Figure 1. Figures 1a, b show non-contact (nc) atomic force microscopy (AFM) images on TiO_2(110) surfaces and Figure 1c an STM image obtained from a TiO_2 film on Ru(0001). Figure 1a shows a well-ordered stoichiometric surface, with broad, atomically flat terraces with a typical width of about 100 nm separated by monolayer steps, which is obtained by annealing in air at 950 °C (as outlined in ref. [24]). Figure 1b shows, similar to Figure 1a, a flat surface of a bulk-reduced TiO_2(110) substrate obtained after repeatedly annealing stoichiometric TiO_2(110) in UHV at 730 °C (30 min); however, the step density is clearly enhanced. As known from reducible metal oxides, an annealing process under vacuum conditions causes mainly a loss of oxygen in the surface and subsurface region of the substrate.[25] In the case of TiO_2(110), it leads to the presence of Ti interstitials (i.e., Ti^{n+} cations at interstitial sites). The latter defects can easily diffuse in reduced TiO_2(110) and are made responsible for many interesting phenomena of this material.[15,25] Figure 1c displays an STM image obtained from an in situ prepared TiO_2(110)/Ru(0001) film (thickness: 10 ML) which shows titania islands of different heights (diameter: 20–30 nm) with atomically flat and well-ordered TiO_2(110) surfaces on top.[26] X-ray photoelectron spectroscopy (XPS) data do not reveal any Ru-related peaks and confirm that the whole Ru surface is covered with TiO_2.[26,27]

Additional cross-section images using high-resolution transmission electron microscopy (HR-TEM) on both types of TiO_2(110) supports show planar surfaces with a small roughness. In contrast to the stoichiometric TiO_2(110) substrate (left column in Figure 2), which nicely shows the periodic rutile structure, the images from the bulk-reduced substrate (right column in Figure 2) display an inhomogeneous structure with many holes and dislocations. Although it is well known that a bulk-reduced TiO_2(110) substrate exhibits defects, mostly oxygen vacancies and Ti^{n+} atoms at interstitial sites in the subsurface region, the observed degree of disorder does not represent the internal structure of such substrates. During the preparation of the sample for cross-section TEM investigations, ion-milling processes (Ar ions with energies up to 5 keV) strongly interact with defects in the crystal and create the hole-like structure (cf. Figure 2) by removing preferentially atoms close to defect sites. However, the surface remains intact and shows a flatness similar to that

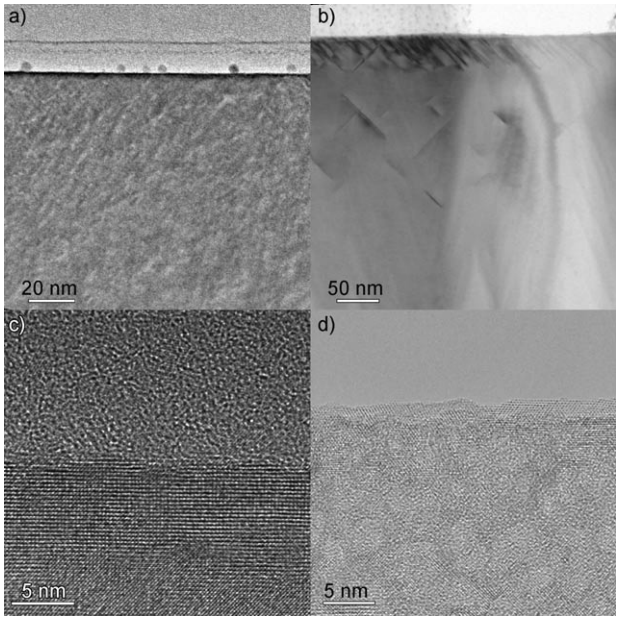

Figure 2. Bright-field overview (a and b) and HR-TEM (c and d) images of the surface of stoichiometic (a, c) and bulk-reduced (b,d) TiO_2(110). The bulk-reduced TiO_2(110) sample shows massive crystalline defects such as holes and dislocations. Image (a) (upper left panel) shows, additionally, Au nanoparticles from a micelle-based deposition process, see. Figure 6.

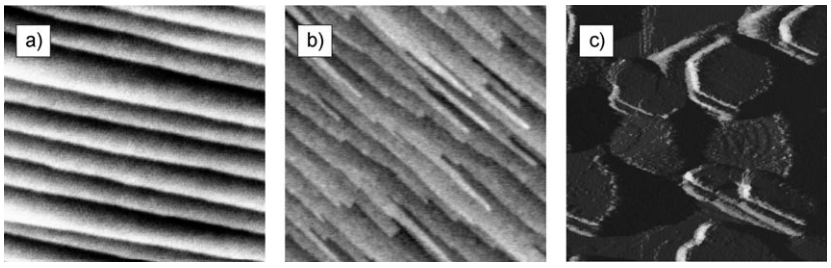

Figure 1. Surface morphology of differently prepared TiO_2 supports: a) stoichiometric TiO_2(110) surface, b) surface of bulk-reduced TiO_2(110) after annealing to 730 °C in UHV (AFM images: 800 nm x 800 nm), c) thin TiO_2 film on Ru(0001) (STM image: 120 nm x 120 nm).

of the stoichiometric sample. The depth of the inhomogeneous defective crystal structure corresponds to the thickness of the reduced TiO_2. This state is determined by the history of the sample and the defect depth increases with time and temperature of the heat treatment starting from stoichiometric rutile substrates.

Au Nanoparticles Produced by Thermal Evaporation on TiO_2 Supports

The CO oxidation reaction on Au/TiO_2 catalysts is characterized by a strong dependence of the catalytic activity with respect to the size of the Au nanoparticles with a maximum at about 3 nm.[8,28] Whereas this value denotes the diameter of (more or less) spherically shaped particles on high surface area materials, it refers to the lateral diameter of Au particles on planar TiO_2 surfaces. The corresponding height of evaporated Au is usually between two and four monolayers. Since the size distribution of thermally evaporated Au islands depends on the substrate and its preparation conditions,[22] this point was investigated in situ for the planar Au/TiO_2 catalysts using AFM [TiO_2(110) substrates] or STM [TiO_2 films on Ru(0001)]. The size and shape of Au nanoparticles strongly depend on the Au coverage: at very low coverage, only mono- or bilayer islands are formed whereas hemispherical objects occur at intermediate Au coverages (0.5 ML), finally reaching a nearly spherical shape at coverages of more than 1 ML.[29] The driving force determining the particle shape is the ratio of the respective surface energies γ of TiO_2 and Au, which favors a 3D growth mode ($\gamma_{TiO2} < \gamma_{Au}$). The height distribution of Au nanoparticles on stoichiometric TiO_2(110) supports has already been investigated in detail using nc-AFM.[30] At a low Au coverage (0.2 ML), most particles have a height of only 1–2 layers (Figure 3 left); the height increases slightly when the system is annealed under UHV conditions to 400 °C for 5 min. More details about the height distribution for different Au coverages and the stability in reactive gases can be found in ref. [31]. The height distribution of Au nanoparticles on bulk-reduced supports, however, shows its maximum around 2–3 layers (Figure 3 center) for a re-oxidized surface with a similar Au coverage. Due to the strong tip convolution, the lateral diameter of the Au nanoparticles cannot be determined using AFM. Analogous investigations were performed on thin TiO_2 films on Ru(0001) by means of STM,[26,27] the results for a coverage of 0.3 ML Au are shown in the right part of Figure 3. The height distribution on the thin films shows a similar behavior as on the TiO_2(110) support when taking into account the slightly higher Au coverage. The STM image clearly shows that most particles are located at

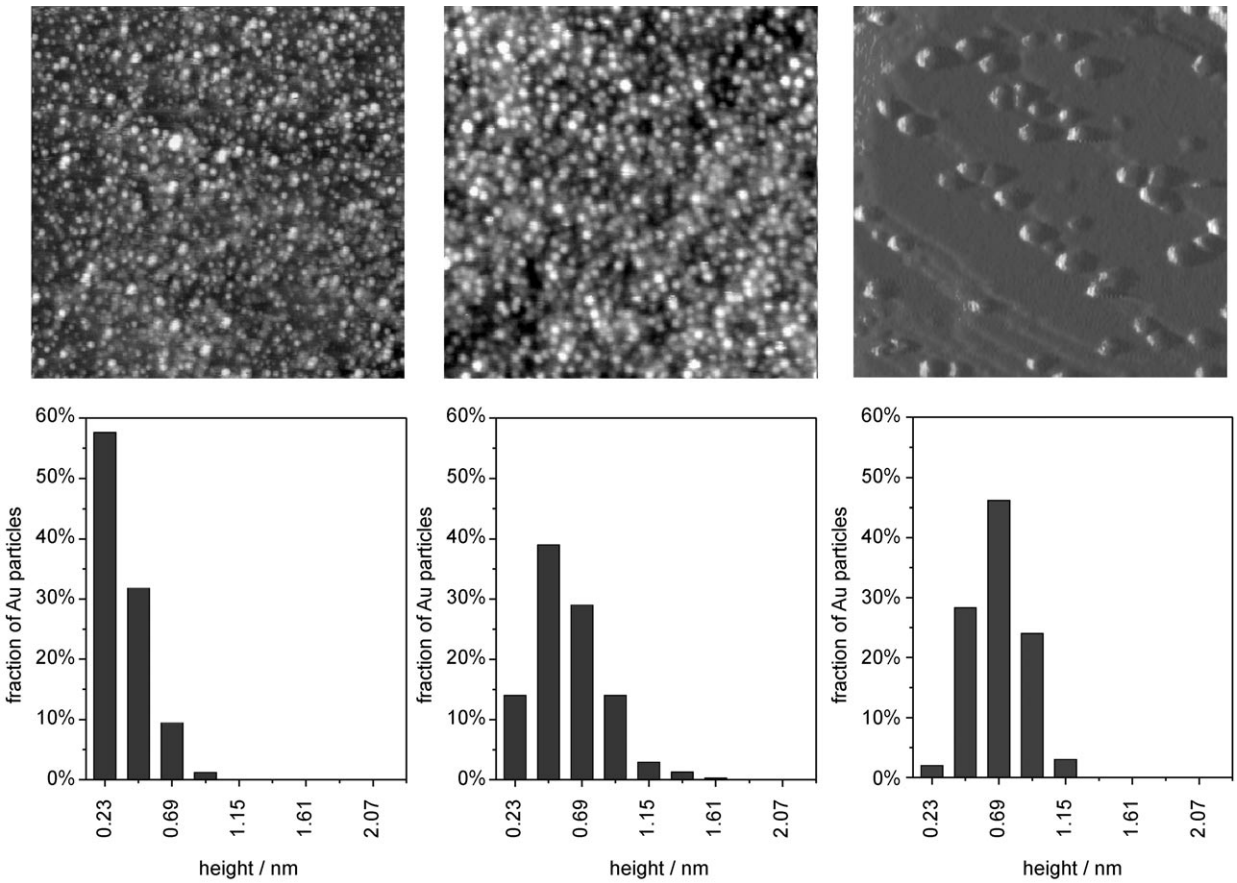

Figure 3. Top: nc-AFM and STM images obtained from different planar Au/TiO_2 model catalysts: left: 0.2 ML Au on fully oxidized TiO_2(110), middle: 0.2 ML Au on bulk-reduced and re-oxidized TiO_2(110), right: 0.3 ML Au on TiO_2/Ru(0001). AFM images: (175 nm × 175 nm), STM image (right part: 50 nm × 50 nm, $U_T = 2.5$ V, $I_T = 562$ pA). Bottom: corresponding Au-particle height distributions.

step edges, only a few particles exist on the flat terraces. In general, particles at step edges are slightly higher than those on the terraces. The typical lateral diameters of the Au nanoparticles are in the order of 2 nm for the Au coverage used in this experiment. Similar to the findings for Au/TiO_2(110) model systems, the size distribution does not change significantly after annealing to 400 °C under UHV conditions, excluding the possibility of considerable sintering under these conditions.[26]

The chemical state of the Au/TiO_2 model catalysts was investigated using XPS. The results of these measurements are displayed in Figure 4, which shows both Ti(2p) and Au(4f) peaks.

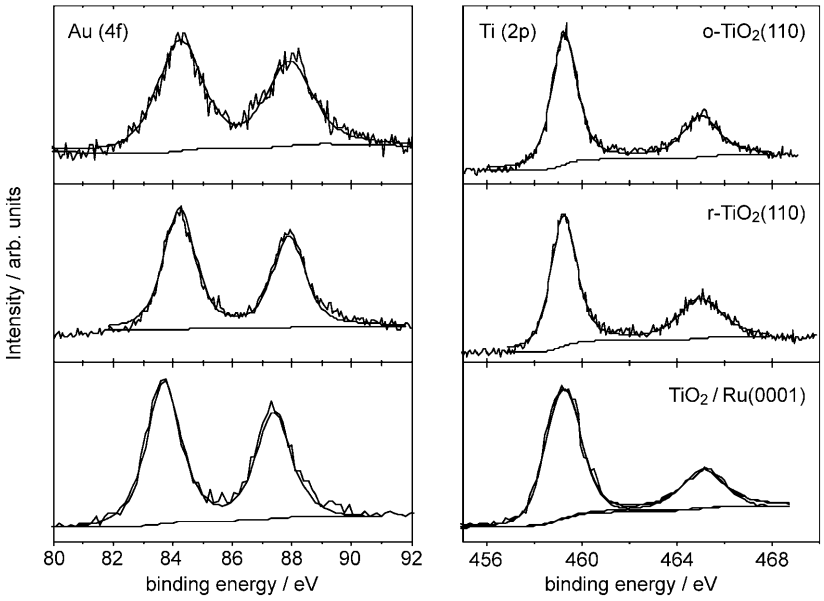

Figure 4. XPS spectra of the Au(4f) peaks (left) and Ti(2p) peaks (right) taken from stoichiometric (top), bulk-reduced (middle) planar Au/TiO_2(110) and Au/TiO_2/Ru(0001) (bottom) model catalysts. Au coverage: 0.2 ML.

The XPS spectra of all the TiO_2 supports show identical binding energies and shapes, which correspond to fully oxidized titania [i.e. Ti^{4+}, Ti($2p_{3/2}$) binding energy reference: 459.2 eV[32]]. This result was expected for the stoichiometric TiO_2(110) support (topmost panel). In the bulk-reduced TiO_2(110) supports, the defect density (oxygen vacancies and Ti interstitials) is below the detection limit of XPS ($\approx$1%) and thus, no energy shift or shoulders occurring from other valences than Ti^{4+} can be detected (middle). Similar to the TiO_2(110) substrates, also the TiO_2 film on Ru(0001) shows Ti(2p) features, which cannot be distinguished from the bulk sample (lower diagram). Analogous to the results of the measurements of the Ti(2p) peaks, also the Au (4f) spectra show for all three types of model catalysts nearly identical results. A feature is observed, which can be fitted by a single set of peaks at the position typical for metallic Au [binding energy (BE) of Au($4f_{7/2}$) peak: 84.0 eV]. The presence of Au oxide species would lead to additional XPS peaks at higher binding energies (e.g., Au^{3+}: BE 85.9 eV), which are not visible in the Au(4f) related data of Figure 4, and can thus be excluded after Au deposition under UHV conditions. Additionally, small peak shifts to higher binding energies (BE) might occur for very small Au particles, usually below 1 nm [as in the case of Au nanoparticles on TiO_2 films on Ru(0001) for an Au coverage of about 0.06 ML[26]]. These XPS BE shifts result from final state effects in photoelectron spectroscopy (i.e., an interaction of the outgoing photoelectron with the positively charged Au after photoexcitation), whereas ionic BE shift are related to initial state effects (BE shifts before photoexcitation). The results presented in Figure 4 demonstrate that the differently prepared TiO_2 supports always lead to metallic Au nanoparticles with similar electronic and chemical properties.

Au Nanoparticles Produced by the Micelle-Based Technique on TiO_2 Supports

Micelle-based planar Au/TiO_2 model catalysts have the advantage of a well-defined narrow particle size distribution and well-defined interparticle distances, which can both be tuned by modifying the type of polymer used for the micelle shell and the metal salt loading.[33] Typical values for particle sizes lie in the range of 2 to 10 nm, interparticle distances can be varied between 25 and 100 nm depending on the particle size. Details on this technique have been described elsewhere.[24,34]

Thus, these hexagonally ordered model systems are extremely well suited to study any structural rearrangement of the Au particles under reaction conditions such as sintering or shape deformations. Such investigations have previously been carried out in different gases.[24]

Figure 5 shows a nc-AFM image of micelle-based Au nanoparticles on a stoichiometric TiO_2(110) support recorded under UHV conditions. The corresponding height distribution obtained by AFM is displayed in the right part with a mean height of (3.1 $\pm$ 0.9) nm. The particle array has a high degree of hexagonal order with a mean interparticle distance of 25 nm. Details regarding the degree of order are published elsewhere.[35] Since AFM can only give reliable information on the height of the nanoparticles, we have additionally analyzed the particles by means of HR-TEM in a new series of experiments.

The left part of Figure 6 displays a high-resolution TEM image of a single Au nanoparticle on fully oxidized TiO_2(110), all particles on the support have been capped in situ with a SiO_2 layer to prevent them from any damage during the TEM preparation steps. To exclude an influence of the SiO_2 capping layer, additional experiments have been performed with other capping materials (e.g., boron nitride). The image shows a spherically shaped Au nanoparticle with nearly equal height

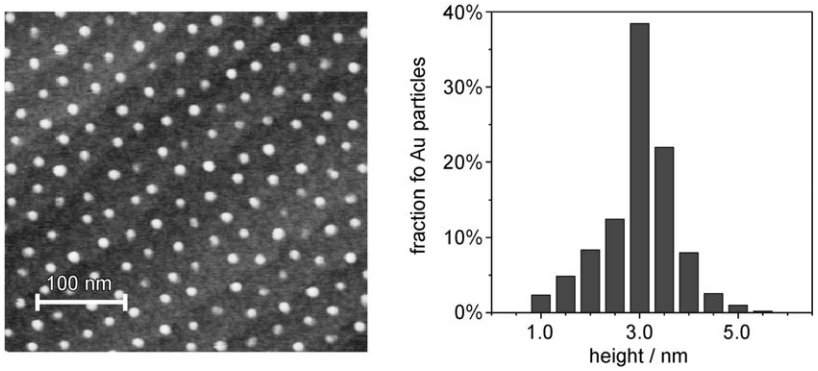

Figure 5. Micelle-based planar $Au/TiO_2(110)$ model catalysts: nc-AFM image (400 nm × 400 nm) (left) and corresponding height distribution evaluated from AFM imaging (right).

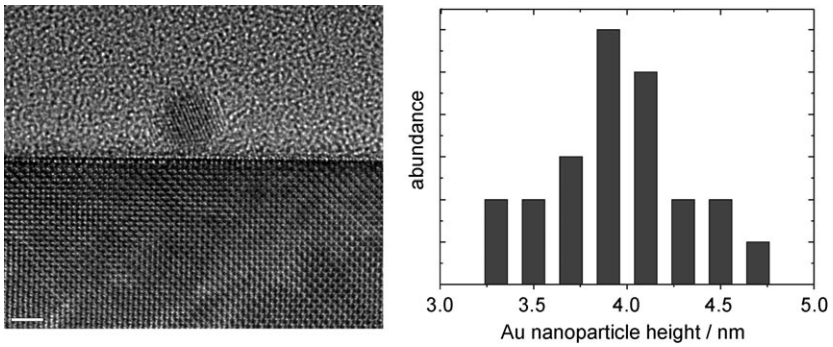

Figure 6. Left: cross-sectional high-resolution TEM image from a single micelle-based Au nanoparticle on $TiO_2(110)$; scale bar: 2 nm. Note: Figure 2 (upper left panel) shows an area with several Au nanoparticles. Right: Height distribution of micelle-based Au nanoparticles (mean diameter: 3.8 nm) on $TiO_2(110)$.

and diameter. The mean height (3.9 ± 0.4) nm and the mean width (3.8 ± 0.8) nm of the Au nanoparticles, see right part of Figure 6, has been determined from a series of HR-TEM images of different Au nanoparticles. Note that the height distribution for micelle-based Au nanoparticles is much narrower compared to thermally evaporated Au particles of a respective size.

As a consequence of the spherical shape, the interface between the $TiO_2(110)$ support and the Au nanoparticles is very small and thus, the bonding of the particles to the TiO_2 surface is rather weak; in fact, the Au particles can easily be removed at air by wiping. Although micelle-based planar $Au/TiO_2(110)$ catalysts represent nearly perfectly ordered model systems, their application as catalysts has to be shown. Besides the very low Au coverage, which already requires a modified detection technique with higher sensitivity, the small perimeter at the interface might cause additional problems in the CO oxidation reaction. Haruta and co-workers suggested a model that scales the catalytic activity of Au/TiO_2 catalysts with the length of the perimeter of the Au nanoparticles at the interface, where the crucial step of the CO oxidation reaction should take place.[36] Measurements on the catalytic activity of these micelle-based Au nanoparticles are currently underway.

Due to the misfit of the respective lattice constants of TiO_2 (a, b: 0.295 nm, c: 0.459 nm) and Au (0.408 nm) in combination with the extremely small interface, one would not expect an epitaxial order of the Au nanoparticles on $TiO_2(110)$. Diffraction experiments performed at individual Au nanoparticles during the HR-TEM study confirm a statistical ordering. Similar results have been obtained in in situ reflection high-energy electron diffraction (RHEED) experiments; annealing up to 400 °C did not show any changes. Shibata et al.[37] also found an incoherent-type hetero-interface for particles larger than 2 nm.

2.2. Catalytic Activity of Planar Au/TiO_2 Model Catalysts

The catalytic properties of the model catalysts for the CO oxidation were investigated in two different reactors: 1) a home-built batch reactor equipped with a quadrupole mass spectrometer (QMS)[38] (used for the $Au/TiO_2/Ru$ samples) and 2) the microflow reactor described in the Experimental Section. In the first reactor, turn-over frequencies (TOF) of about 0.14 ± 0.04 site^{-1} s^{-1} have been observed for Au nanoparticles with different sizes on TiO_2 films (initial Au coverage: ranging from 0.2 to 0.6 ML) at 80 °C[27,39,40] (total pressure: 20 mbar, $CO:O_2 = 2:1$). This type of model catalysts [0.5 ML Au on TiO_2 films on Ru(0001)] has also been investigated in the microflow reactor and a CO_2 concentration of (3.3 ± 0.2) % was measured in the gas stream behind the reactor. From the CO_2 concentration, we calculate the corresponding TOF (0.16 ± 0.01 site^{-1} s^{-1} at 60 °C), which is in good agreement with the result obtained on TiO_2 films on Ru(0001) in the batch reactor. The results from other measurements on planar $Au/TiO_2(110)$ are compared to this sample which serves as a reference.

The TOF measured from Au nanoparticles (similar Au coverage and similar Au size distribution) on a stoichiometric and nearly defect-free $TiO_2(110)$ substrate, however, is about one order of magnitude smaller than that of the planar Au/TiO_2 catalyst on Ru(0001). The respective CO_2 conversion rate is within the QMS background signal, which is caused by CO_2 production in the presence of the reaction gases (CO and O_2) at the hot filament of the QMS; the TOF can be estimated to be smaller than 0.003 site^{-1} s^{-1}. Contrary to this finding, measurements of similarly prepared planar $Au/TiO_2(110)$ catalysts on

bulk-reduced supports show CO_2 conversion rates well above the detection limit, but roughly a factor of five below the value obtained from Au/TiO_2 film/Ru(0001) model catalyst (see Table 1). Since the particle size distribution does not vary significantly from those on stoichiometric supports, as shown in Figure 3, the turnover frequency directly scales with the conversion rate and has been determined to be 0.034 ± 0.010 site^{-1} s^{-1}. These experiments were repeated several times with nearly identical results.

Table 1. Turn over frequency (TOF) obtained from different planar Au/TiO_2 model catalysts at 60 °C.

	TiO_2/Ru(0001) (batch reactor)	oxidized TiO_2(110)	reduced TiO_2(110)	TiO_2/Ru(0001)
Au coverage [ML]	0.2–0.8	0.5 ± 0.05	0.5 ± 0.05	0.5 ± 0.05
CO_2 concentration	–	< 0.05 %	(0.7±0.2) %	(3.3±0.2) %
TOF [site^{-1} s^{-1}]	0.14 ± 0.04 (80 °C)	< 0.003	0.034 ± 0.010	0.16 ± 0.01

The experimental results shown above strongly suggest an important—if not critical—influence of the TiO_2 support on the catalytic activity, although often other criteria are discussed in the literature (size effects, extraordinary activity of Au bilayer systems,[9] presence of oxidized Au species[6]). Goodman and co-workers[41] outlined the importance of reduced titania supports (or at least TiO_2 surfaces with many oxygen defects): 1) reduced titania surfaces enable the adsorption of oxygen and 2) the presence of Au nanoparticles on surface defects leads to a stronger interaction, which results in flatter particles and a partial negative charge on Au due to charge transfer from oxygen vacancies.

Recently, Wahlström et al.[42] showed, by means of STM studies, that oxygen vacancy defects on reduced TiO_2(110) surfaces are mobile, assemble under Au nanoparticles, and the high number of statistically distributed vacancies on the native surface decrease dramatically after Au evaporation and particle formation. At low Au coverages, the authors were able to correlate a mean number of vacancies to the number of atoms in Au nanoparticles. Moreover, Rodriguez et al.[43] proposed that the presence of Au on reduced supports i) stabilizes oxygen vacancies at the surface and ii) modifies the exchange rate of oxygen defects between the surface and the bulk to an extent that leads to a stabilization of the Au nanoparticles (i.e., more oxygen vacancies in surface position on the cost of subsurface vacancies). It is important to note that a small amount of the negative charge from oxygen vacancies, although delocalized to a certain extent, can be transferred to the Au nanoparticles,[21,43,43] a process that is not possible for stoichiometric TiO_2(110) samples. This additional charge may partly be located at the Au–TiO_x interface.[25] Depending on the size of the Au nanoparticles and the amount of charge transfer, this effect could be visible in infrared (IR) spectra of CO adsorbed on these particles by shifts to higher or lower wavenumbers depending on the sign of the charge.[11] Whereas the CO stretching frequencies on single-crystal Au surfaces are located at 2124 cm^{-1}, bilayer Au particles on reduced TiO_2(110) supports give rise to slightly shifted CO stretching frequencies (around 2110 cm^{-1}) and thus, these Au nanoparticles are considered as electron-rich $Au^{\delta-}$ species.[13]

In situ IR investigations on our Au/TiO_2/Ru(0001) model catalysts[40] during exposure to reactive gases (pure CO and CO/O_2 gas mixtures) mainly showed CO stretching frequencies around 2110 cm^{-1}. Only at higher CO pressure (50 mbar), an additional peak was observed at 2060 cm^{-1}, which remained after decreasing the CO pressure. This band was attributed to a flattening of the Au nanoparticles on more strongly reduced titania films, according to the reducing influence of CO. The process is reversible when exposing the system to oxygen. However, the influence of such effects on the catalytic activity is still not clear. Unfortunately, similar experiments on TiO_2(110) supports are not possible in the microflow reactor, since the surface is not directly accessible to IR spectroscopy.

Recent publications mention that surface oxygen vacancies, which are often made responsible for the catalytic activity in Au/TiO_2 catalysts, might only play a minor role in catalysis.[13,14] Oxygen vacancies are easily filled in the presence of reactive gases (such as O_2 and H_2O) and, from an energetic point of view, they seem to be less favorable to promote the CO oxidation reaction, as discussed in the literature before. Several publications[12,13,44,45] focus on the influence of Ti interstitials which are present when TiO_2(110) supports are annealed at higher temperatures in UHV. These defects can easily move in TiO_2 at elevated temperatures and preferentially diffuse to the surface when oxygen is present in the gas phase. As a consequence, several authors observed the formation of new TiO_2 layers on top of the existing TiO_2(110) sample at temperatures above 200 °C and an O_2 pressure of 10^{-6} mbar.[15,46–48] The influence of these additional layers on the catalytic activity is still under discussion.[16,47]

Wendt et al.[12] proposed that Ti interstitials in the near subsurface regime should promote the catalytic activity of planar Au/TiO_2 model catalysts by lowering the energetic barrier of the CO oxidation. The presence of surface vacancies alone (e.g., created by sputtering with Ar ions) should not lead to enhanced conversion rates, but together with Ti interstitials, it should again have a preferential influence on the catalytic activity. First results from our group confirm these predictions: Kielbassa[31] found that the CO_2 conversion rate measured on a stoichiometric TiO_2(110) support with a high number of oxygen vacancies is nearly equal to a sample without surface defects. On the other hand, Au/TiO_2 model catalysts with bulk-reduced TiO_2 supports clearly show an enhanced TOF compared to stoichiometric supports. This is a clear indication that the presence of subsurface oxygen defects caused by the segregation of Ti interstitials has a strong influence on the catalytic activity.

3. Conclusions

Herein, we have presented experimental results on differently prepared planar Au/TiO_2 model catalysts. A direct comparison of stoichiometric and reduced TiO_2(110) supports shows that the catalytic activity of these model systems strongly depends on the preparation of the underlying support. Au nanoparticles created under UHV conditions on a stoichiometric support have a very low catalytic activity which is about one order of magnitude below the respective value for a reduced TiO_2(110) support. According to our results, surface oxygen vacancies, which have often been made responsible for the higher activity on reduced substrates, cannot solely explain the different catalytic activity and thus seem to play only a minor role in this process. The segregation of Ti interstitials from TiO_2 bulk regions to subsurface regions in the presence of reactive gases and subsequent chemical processes at the TiO_2 surface and Au–TiO_2 interface are expected to have a high impact on the catalytic activity, most likely by lowering energetic barriers for the CO oxidation. Our experimental results are generally in agreement with the recently published model calculations regarding the influence of Ti interstitials by Wendt et al. and confirm the minor importance of oxygen vacancies at reduced surfaces. The size or the height of the Au nanoparticles on the titania surface might have an additional influence on the reactivity; however, this was not the subject of the study presented here.

Experimental Section

Most of the planar Au/TiO_2(110) model catalysts were prepared by thermal evaporation of Au at room temperature (RT) in a UHV chamber and afterwards characterized in situ using a home-built nc-AFM[49] and an XPS equipment. The preparation procedure for fully oxidized TiO_2(110) crystals (TBL Kelpin, one side polished, 10 mm × 10 mm × 1 mm) is given in ref. [30].

For obtaining bulk-reduced TiO_2(110) substrates, clean and used bulk-reduced supports were always annealed two times in UHV to 730 °C for 30 min and sputtered with Ar ions (600 V, 30 min, 3 μA) in between. New samples were found to show reproducible reaction rates after at least six cycles of annealing and sputtering. It is important to mention that the temperature has to be increased slowly to avoid damages in the supports. Moreover, the temperature of 730 °C has to be controlled carefully for obtaining reproducible results, since the concentration of defects in the samples scales with an Arrhenius law. The used samples were usually sputtered for 1.5 h to remove the Au nanoparticles before starting the annealing procedure. Before evaporating Au under UHV conditions, the support was checked with XPS for cleanliness. When contaminations such as Si, C, and Ca were detected, the procedure was repeated until the surface was free from contaminations in the XPS spectrum.

For the preparation of the Au/TiO_2 film/Ru(0001) model catalysts, firstly a fully oxidized film (thickness ≈ 10 ML) was prepared on Ru(0001) by Ti deposition in an O_2 atmosphere and subsequent annealing in O_2. Afterwards, Au was deposited again, at RT, on the films (details are described in ref. [26]). The structural and chemical/electronic properties of this model catalyst system were determined by STM and XPS measurements.

Micelle-based Au/TiO_2(110) model catalysts were prepared using reverse micelles. Commercial PS[312]-b-P2VP[74] diblock-copolymers (Polymer Source Inc.) form spherical micelles in water-free toluene at a concentration of 5 mg mL^{-1}.[24] The numbers in brackets reflect the average number of monomer units in the polymer. After one week of stirring at ambient temperature, $HAuCl_4$ salt was added as Au nanoparticle precursor. The salt totally dissolved into the hydrophilic cores of the reverse micelles within a couple of days. Fully oxidized, atomically flat rutile TiO_2(110) substrates were dipped into the solution and emerged at a constant velocity of 15 mm min^{-1}.[34,50] Here, a monolayer of Au-salt-loaded micelles was deposited on the rutile substrates. By means of oxygen radio-frequency (rf) plasma treatment (13.6 MHz, 50 W, 5 Pa, 300 K), the polymer was completely etched within 30 min, thereby forming well-separated Au nanoparticles. In the present case, the procedure led to particles with a mean diameter of 3 nm at a mean interparticle distance of 25 nm, which is largely determined by the length of the polymer (for details, see ref. [24]).

Generally, the samples were transferred in situ into a UHV-compatible reaction cell attached to the main UHV preparation and characterization chamber (micelle-based samples must, of course, first be transported under ambient conditions into the UHV system). The home-built microflow reactor (volume ≈ 2 μL)[31] was used for the characterization of the activity of the Au/TiO_2(110) model catalysts in CO oxidation. The gas composition used in the experiments presented here consists of 6.7% CO and 3.3% O_2 in 170 mbar Ar, the chemical composition (ratio of CO to O_2) of the gases was varied to obtain the highest CO_2 conversion rates.

The analysis of the product gases was performed in a quadrupole mass spectrometer (QMS) located in a different UHV chamber. The QMS was connected to the reactor by a thin fused silica capillary, which adjusted the gas flow to about 1 Nμl min^{-1}; details about the reactor are given in ref. [31]. To reduce the inevitable CO_2 background production at the QMS filament in the presence of the reaction gas mixture of CO and O_2, an yttrium-oxide-based filament was used, which reduces the CO_2 background by about one order of magnitude when compared to a tungsten filament. The error bar in the CO_2 concentration was found to be ±0.2% due to statistics and the CO_2 background signal.

While for AFM and STM no additional surface treatments were needed, transmission electron microscopy (TEM) investigations of cross-sectioned samples demanded a special procedure. The samples were cut into stripes, glued face-to-face, and embedded into 3 mm Ti grids. Then, these sandwiches were grinded, dimpled, and polished down to a thickness of about 5 μm. Low-angle (< 8°) Ar-ion etching (2 to 5 keV) was finally applied until electron transparency was reached (sample thickness < 100 nm). Since Au nanoparticles do not stick very well on TiO_2 surfaces, a thin film of SiO_x was deposited onto these samples prior to the mechanical treatment to cover the nanoparticles and thus avoid unwanted damage during thinning. The TEM investigations were carried out using an FEI Titan 80–300 microscope operating at 300 kV, equipped with an imaging side aberration corrector. The aberrations of the objective lens were corrected up to a phase plate of 20 mrad (corresponding nominal point resolution ≤ 0.1 nm). High-resolution images were recorded on a slow-scan CCD camera (Gatan Ultrascan 1000).

Acknowledgements

We gratefully acknowledge financial support by the collaborative research center (Sonderforschungsbereich 569) of the Deutsche Forschungsgemeinschaft and a grant from the Landesgraduierten-Stipendium Baden Württemberg for (M.E.). We are grateful to L. Han (Ulm Univ.) for Au nanoparticle preparation by reverse micelles, S. Grözinger and V. Binder (Ulm Univ.) for supporting TEM sample preparation. A part of the structural analysis of Au/TiO_2/Ru(0001) was performed by Z. Zhao during his PhD thesis at the Institute of Surface Chemistry and Catalysis, Ulm Univ. (now: University of Lanzhou, China).

Keywords: electrochemistry · gold · model catalysis · oxidation · TiO_2

[1] M. Haruta, N. Yamada, T. Kobayashi, S. Iijima, *J. Catal.* **1989**, *115*, 301 – 309.
[2] R. Meyer, C. Lemire, S. K. Shaikhutdinov, H.-J. Freund, *Gold Bull.* **2004**, *37*, 72 – 124.
[3] G. C. Bond, C. Louis, D. T. Thompson, *Catalysis by gold*, Imperial College Press, London, **2006**.
[4] N. Weiher, E. Bus, L. Delannoy, C. Louis, D. E. Ramaker, J. T. Miller, J. A. van Bokhoven, *J. Catal.* **2006**, *240*, 100 – 107.
[5] N. Weiher, A. M. Bessley, N. Tsapatsaris, L. Delannoy, C. Louis, J. van Bokhoven, S. L. M. Schroeder, *J. Am. Chem. Soc.* **2007**, *129*, 2240 – 2241.
[6] J. Guzman, B. C. Gates, *J. Am. Chem. Soc.* **2004**, *126*, 2672 – 2673.
[7] M. P. Casaletto, A. Longo, A. Martorana, A. Prestianni, A. M. Venezia, *Surf. Interface Anal.* **2006**, *38*, 215 – 218.
[8] M. Valden, X. Lai, D. W. Goodman, *Science* **1998**, *281*, 1647 – 1650.
[9] M. S. Chen, D. W. Goodman, *Science* **2004**, *306*, 252 – 255.
[10] M. M. Schubert, S. Hackenberg, A. C. van Veen, M. Muhler, V. Plzak, R. J. Behm, *J. Catal.* **2001**, *197*, 113 – 122.
[11] M. Chen, D. W. Goodman, *Acc. Chem. Res.* **2006**, *39*, 739 – 746.
[12] S. Wendt, P. T. Sprunger, E. Lira, G. K. H. Madsen, Z. Li, J. Ø. Hansen, J. Matthiesen, A. Blekinge-Rasmussen, E. Lægsgaard, B. Hammer, F. Besenbacher, *Science* **2008**, *320*, 1755 – 1759.
[13] G. Madsen, B. Hammer, *J. Chem. Phys.* **2009**, *130*, 044704.
[14] J. G. Wang, B. Hammer, *Top. Catal.* **2007**, *44*, 49 – 56.
[15] P. Stone, R. A. Bennett, M. Bowker, *New J. Phys.* **1999**, *1*, 8.
[16] K. T. Park, V. Meunier, M. H. Pan, W. A. Shelton, N. Yu, E. W. Plummer, *Surf. Sci.* **2009**, *603*, 3131 – 3135.
[17] L. M. Molina, M. D. Rasmussen, B. Hammer, *J. Chem. Phys.* **2004**, *120*, 7673 – 7680.
[18] G. Lu, A. Linsebigler, J. T. Yates, *J. Chem. Phys.* **1995**, *102*, 4657 – 4662.
[19] M. D. Rasmussen, L. M. Molina, B. Hammer, *J. Chem. Phys.* **2004**, *120*, 988 – 997.
[20] Z.-P. Liu, X.-Q. Gong, J. Kohanoff, C. Sanchez, P. Hu, *Phys. Rev. Lett.* **2003**, *91*, 266102.
[21] K. Okazaki, Y. Morikawa, S. Tanaka, K. Tanaka, M. Kohyama, *Phys. Rev. B* **2004**, *69*, 235404.
[22] T. Okazawa, M. Kohyama, Y. Kido, *Surf. Sci.* **2006**, *600*, 4430 – 4437.
[23] S. C. Parker, A. W. Grant, V. A. Bondzie, C. T. Campbell, *Surf. Sci.* **1999**, *441*, 10 – 20.
[24] S. Kielbassa, A. Häbich, J. Schnaidt, J. Bansmann, F. Weigl, H.-G. Boyen, P. Ziemann, R. J. Behm, *Langmuir* **2006**, *22*, 7873 – 7880.
[25] Q. Fu, T. Wagner, *Surf. Sci. Rep.* **2007**, *62*, 431 – 498.
[26] Z. Zhao, T. Diemant, D. Rosenthal, K. Christmann, J. Bansmann, H. Rauscher, R. J. Behm, *Surf. Sci.* **2006**, *600*, 4992 – 5003.
[27] Z. Zhao, PhD thesis, Ulm University, Ulm **2006**.
[28] G. R. Bamwenda, S. Tsubota, T. Nakamura, M. Haruta, *Catal. Lett.* **1997**, *44*, 83 – 87.
[29] U. Diebold, *Surf. Sci. Rep.* **2003**, *48*, 53 – 229.
[30] S. Kielbassa, M. Kinne, R. J. Behm, *J. Phys. Chem. B* **2004**, *108*, 19184 – 19190.
[31] S. Kielbassa, PhD thesis, Ulm University, Ulm **2008**.
[32] D. Gonbeau, C. Guimon, G. Pfister-Guillouzo, A. Levasseur, G. Meunier, R. Dormoy, *Surf. Sci.* **1991**, *254*, 81 – 89.
[33] A. Ethirajan et al., *Adv. Mater.* **2007**, *19*, 406 – 410.
[34] G. Kästle et al., *Adv. Funct. Mater.* **2003**, *13*, 853 – 861.
[35] J. Bansmann, S. Kielbassa, H. Hoster, F. Weigl, H.-G. Boyen, U. Wiedwald, M. M. Möller, P. Ziemann, R. J. Behm, *Langmuir* **2007**, *23*, 10150 – 10155.
[36] M. Haruta, S. Tsubota, T. Kobayashi, H. Kageyama, M. J. Genet, B. Delmon, *J. Catal.* **1993**, *144*, 175 – 192.
[37] N. Shibata, A. Goto, K. Matsunaga, T. Mizoguchi, S. D. Findlay, Y. Yamamoto, Y. Ikuhara, *Phys. Rev. Lett.* **2009**, *102*, 136105.
[38] Z. Zhao, T. Diemant, T. Häring, H. Rauscher, R. J. Behm, *Rev. Sci. Instrum.* **2005**, *76*, 123903.
[39] T. Diemant, Z. Zhao, H. Rauscher, J. Bansmann, R. J. Behm, *Surf. Sci.* **2007**, *601*, 3801 – 3804.
[40] T. Diemant, Z. Zhao, H. Rauscher, J. Bansmann, R. J. Behm, *Top. Catal.* **2007**, *44*, 83 – 93.
[41] T. V. Choudhary, D. W. Goodman, *Appl. Catal. A* **2005**, *291*, 32 – 36.
[42] E. Wahlström, N. Lopez, R. Schaub, P. Thostrup, A. Rønnau, C. Africh, E. Laegsgaard, J. K. Nørskov, F. Besenbacher, *Phys. Rev. Lett.* **2003**, *90*, 026101.
[43] J. A. Rodriguez, G. Liu, T. Jirsak, J. Hrbek, Z. Chang, J. Dvorak, A. Maiti, *J. Am. Chem. Soc.* **2002**, *124*, 5242 – 5250.
[44] H. Cheng, A. Selloni, *J. Chem. Phys.* **2009**, *131*, 054703.
[45] J. Nowotny, T. Bak, L. R. Sheppard, M. K. Nowotny, *J. Am. Chem. Soc.* **2008**, *130*, 9984 – 9993.
[46] R. A. Bennett, P. Stone, N. J. Price, M. Bowker, *Phys. Rev. Lett.* **1999**, *82*, 3831 – 3834.
[47] K. T. Park, M. Pan, V. Meunier, E. W. Plummer, *Phys. Rev. B* **2007**, *75*, 245415.
[48] M. Li, W. Hebenstreit, L. Gross, U. Diebold, M. A. Henderson, D. R. Jennison, P. A. Schultz, M. P. Sears, *Surf. Sci.* **1999**, *437*, 173 – 190.
[49] J. Wiechers, *PhD Thesis*, Ludwig-Maximilian-Universität, München **1993**.
[50] J. P. Spatz, S. Mößmer, C. Hartmann, M. Möller, T. Herzog, M. Krieger, H.-G. Boyen, P. Ziemann, B. Kabius, *Langmuir* **2000**, *16*, 407 – 415.

Received: December 2, 2009
Revised: March 3, 2010
Published online on April 8, 2010

